International Journal of Hydrogen Energy 90 (2024) 768–774

Contents lists available at ScienceDirect

International Journal of Hydrogen Energy

journal homepage: www.elsevier.com/locate/he

Investigation of steady-state gas diffusion through angled metallised polymer films for applications in fibre reinforced pressure vessels as barrier membranes

Nico Gerster *, Andreas Scherer, Gerrit Rehs, Tobias Dickhut

Composite Materials and Engineering Mechanics, University of the Bundeswehr Munich, Neubiberg, 85577, Bavaria, Germany

ARTICLE INFO

Handling Editor: Dr A Iranzo

Keywords:
Gas diffusion
Pressure vessel
Barrier membrane

ABSTRACT

Pressure vessels used for the storage of hydrogen gas, particularly carbon-fibre reinforced pressure vessels (CPVs), must demonstrate sufficient leak tightness. Currently, this is achieved by costly metallic liners which come at a weight disadvantage compared to CPVs. Therefore, novel concepts for designing CPVs with low permeation characteristics are of high interest for various industrial applications. In this paper, a new concept is proposed based on overlapping intersections of metallised polymer films. Manufacturing trials are carried out on a laboratory scale to demonstrate the feasibility of a new barrier membrane design that can also be integrated into the winding process of CPVs. An efficient analytical model, as well as finite element simulations, are compared against experimental findings for the permeation of Helium. The findings indicate significant promise for implementing the barrier concept in CPVs, with tests and models demonstrating an over 1000 - fold decrease in the permeability of the barrier membrane compared to pure polymer, even when utilizing unoptimized tape materials. Reductions by a factor of over 10 000 are possible with material optimisation.

1. Introduction

The storage of hydrogen can be achieved in three forms: in liquid form at cryogenic conditions, as a highly pressurised gas or in the form of hydrides [1]. Of these three options cryogenic and high-pressure storage solutions have already been well established. Particularly high-pressure storage of hydrogen is considered to be the most suitable form of storage for near future use of hydrogen on a large scale [2].

Carbon fibre-reinforced pressure vessels are deemed a key technology for hydrogen storage in both the aerospace and automotive markets due to the associated weight savings [2]. One particular problem arising from high-pressure storage is the potential for gas leakage through diffusion, posing a significant safety concern, as well as introducing further application dependant concerns, resulting in functional failure.

Impermeable propellant tanks in the aerospace and automotive industry, designed for the storage of high-pressure hydrogen, can only be realised as fully metallic or as composite overwrap pressure vessels with a metallic liner [3,4]. Liner-less fibre-reinforced composites are prone to the formation of small cracks under load, which can significantly influence the leakage of hydrogen [5] and furthermore offer a diffusion path through the polymeric matrix system itself. While metallic liners are effective, they often come at a significant cost and weight disadvantage [6,7].

In this context, polymeric liners have garnered attention as a more feasible alternative, particularly for applications involving large tanks, scalable tank concepts, or industries with stringent cost and mass considerations [8,9]. However, it is important to note that polymeric liners have limitations when it comes to achieving the same level of impermeability as metals, a crucial requirement for meeting various technical standards [10,11]. Nonetheless, extensive research is being conducted to assess the performance of polymers for applications in pressure vessels [12–15]. Despite this, no definitive solution to the elevated permeability of polymeric liners has been established, in particular for strict leak tightness requirements.

In [16] the permeability of membrane materials loaded with high aspect ratio flakes was explored, demonstrating that an increased diffusion path and a reduction in the free volume significantly reduces the permeability. This was further confirmed in Refs. [17,18]. Similarly, in Ref. [19] improved permeability characteristics were achieved using nanosheet filler materials. In addition, the permeation characteristics based on the random or structured orientation of these nano-fillers were investigated. In Ref. [20] multiple approaches to barrier membranes

* Corresponding author.
E-mail address: nico.gerster@unibw.de (N. Gerster).

https://doi.org/10.1016/j.ijhydene.2024.09.136
Received 22 May 2024; Received in revised form 8 September 2024; Accepted 11 September 2024
Available online 8 October 2024

were reviewed based on crack stoppers and a tortuous diffusion path.

In this publication, multilayer films in tape form are investigated as a barrier membrane concept for carbon fibre pressure vessels. These tapes are to be integrated in a filament winding process to satisfy the permeability requirements of pressure vessels.

Instead of incorporating flakes, in this study impermeable layers span the entire width of individual tapes, forming a sandwich arrangement of permeable material on the top and bottom, with an impermeable layer in the middle. These tapes are to be wrapped in an overlapping manner, thereby having a diffusion path that is sufficiently long in a thin membrane. These raw materials have already found widespread application in the packaging field [21] and have demonstrated their ability to prevent the permeation of oxygen and water vapour [22].

The paper aims to demonstrate the working principle of the approach and support it with equations and simulations to predict the permeability of the barrier membrane. Additionally, the paper aims to demonstrate the practical applications of low leak rate barrier membrane systems in aerospace and automotive hydrogen pressure vessels. Furthermore, we highlight potential optimisation avenues of the barrier membrane, presenting opportunities for further refinement and enhancement to maximize performance and utility in real-world scenarios.

The chosen approach shows significant advantages over conventional plastic liners, such as those used in type IV tanks, and flake loaded membranes. The process is aimed at using standard materials and processes and should ensure cost-efficient tank production with existing production facilities in the future. In addition, the in-situ production of the barrier membrane for each individual pressure vessel directly facilitates flexibility and scalability, allowing seamless adaptation to different tank sizes and industrial applications, thus easily meeting different requirements. Special expensive moulding tools, such as those required for plastic liners, are not needed.

A novel analytical model is constructed to allow fast predictions of the permeability and gas diffusion process. This is accompanied by finite element simulations to verify the model and to provide a deeper understanding of the diffusion process. Lastly, experimental tests are performed to validate the model and simulation results.

2. Novel analytical model for permeability prediction of barrier membrane

The one-dimensional, steady-state diffusion of gases through a membrane, based on a pressure differential, is governed by Fick's first law [23]. There the flux is dependent on the concentration gradient across the membrane, where the concentration c of the permeating gas in the membrane is expressed in $\mathrm{mbar}\cdot l/\mathrm{mm}^{-3}$, and the diffusivity D, expressed in mm^2/s.

$$J = P\frac{dc}{dx} \tag{1}$$

The relation between the concentration and pressure of the gas is often assumed to follow Henry's law, defining a linear relation via the solubility of the gas [24]. This gives rise to the steady-state solution for the leak rate Q_0:

$$Q_0 = P\frac{\Delta p}{\Delta x}A \tag{2}$$

Here P, expressed in $\mathrm{mbar}\cdot l/\mathrm{s}\cdot\mathrm{bar}^{-1}\cdot\mathrm{mm}^{-1}$, is the permeability, being the product of the diffusivity D and solubility S according to Henry's Law, Δp is the pressure difference across the membrane, Δx is the membrane thickness, and A is the surface area of the membrane.

In this paper, it is assumed to have a tri-layer layup consisting of two permeable outer layers, made of a thermo-plastic polymer, and an impermeable middle layer, made of metal. These laminate polymer tapes are layered over each other with an overlap ratio R. The aim is to explore the gas permeation effects at these overlapping interfaces and to determine the feasibility of designing carbon fibre pressure vessels with such a barrier layer concept.

Each 'tape' has a width b, thickness t and a resulting aspect ratio $\mathscr{AR} = b/t$. The overlap ratio R defines the level of overlap at the interfaces as a fraction of the total tape width. An idealised arrangement of these tapes is shown in Fig. 1. From this arrangement, an induced angle α can be determined (Eq. (3)). Under the assumption that the tapes have a high aspect ratio, the triangular notches are negligible in size.

The induced angle α is inversely proportional to the overlap ratio R and the aspect ratio $\mathscr{AR}$. The true behaviour will likely result in kinking of the tapes forming an S shape as opposed to remaining flat, particularly for low overlap ratios. However, due to the high aspect ratio of the tapes, the idealised and true geometries are sufficiently similar. It should also be noted that although all overlap ratios $0 \leq R \leq 1$ are theoretically possible, the edge cases are not of significant interest due to limitations arising in the manufacturing process.

$$tan(\alpha) = \frac{t}{(1-R)b} = ((1-R)\mathscr{AR})^{-1} \tag{3}$$

It is assumed that the flux vector **J** can be divided into its components J_γ and J_ξ in the local coordinate system, and are governed by Eq. (1), with the membrane thickness being replaced by appropriate diffusion paths for each coordinate axis. As the permeating gas passes through the entire membrane in either coordinate component, the global boundary conditions in the x-direction and hence the difference in concentration across the membrane hold, resulting in Eq. (4).

$$J_\gamma = D_\gamma\frac{\Delta c}{Rb} \tag{4a}$$

$$J_\xi = D_\xi\frac{\Delta c}{\Delta x}cos(\alpha) \tag{4b}$$

When Henry's law is substituted to replace the concentration gradient, the diffusivity is also replaced by the permeability in the γ and ξ coordinates respectively. The flux in the x-direction is derived by transforming the flux components from the local coordinate system to the global system and summing up the components in the x-direction.

$$J_x = J_\gamma\sin(\alpha) + J_\xi\cos(\alpha) \tag{5a}$$

$$= P_\gamma\frac{\Delta p}{Rb}\sin(\alpha) + P_\xi\frac{\Delta p}{\Delta x}\cos^2(\alpha) \tag{5b}$$

The solution for the flux in the x-direction J_x can be equated to the mean flux through a homogeneous material. This allows the permeability P_x to be derived for the layered tapes. Given that $P_\gamma \gg P_\xi$ the permeability P_x will be dominated by the polymer properties and the overlap ratio R.

$$P_x = \Delta x\left(P_\gamma\frac{\sin(\alpha)}{Rb} + P_\xi\frac{\cos^2(\alpha)}{\Delta x}\right) \tag{6}$$

Under the assumption that P_ξ is negligible, the mean permeability P_x

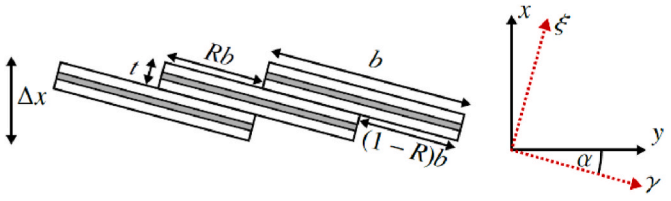

Fig. 1. Idealised model of overlapping tapes (boxed in black) with induced angle α. Each tape is composed of impermeable metal (grey) and permeable polymer (white). The global x-y and local γ-ξ coordinates, inclined at the angle α, are shown.

is at a local maximum when $R = 0$, where the diffusion path is minimal, or $R = 1$, where the ratio of membrane thickness to diffusion path length approaches 1. The minimum is a function of the tape and membrane geometries near $R \approx {}^{1}/_{3}$ for high aspect ratios. However, as the permeability is inversely proportional to the aspect ratio $\mathscr{AR}$, considerable reductions in the permeability can be achieved for a wide range of overlap ratios.

$$P_x \propto \frac{1}{\mathscr{AR}} \frac{\Delta x}{Rb(1-R)}$$

2.1. Membrane thickness

Due to the overlapping nature of the tapes, there is also an influence on the membrane thickness Δx.

$$\Delta x = b\sin(\alpha) + t\cos(\alpha) \tag{7}$$

As the tapes are rectangular when cut, the triangular notches are filled with polymeric material during the consolidation phase. This however means that the induced angle α, the tape thickness t and the polymer volume fraction ν_P are not conserved. Consequently, these properties must be redetermined with the compression. For this the conservation of the polymer and metal phases are used, where variables with an asterisk (*) indicate after compression:

$$bt\nu_P = t^* \nu_P^* b + (1-R) b t^*$$

$$t(1-\nu_P) = t^*\left(1-\nu_P^*\right)$$

This gives the new tape thickness t^* and polymer fraction ν_P^*:

$$t^* = \frac{t}{2-R}$$

$$\nu_P^* = 1 - (2-R)(1-\nu_P)$$

From here a new induced angle α^* can be derived. These new parameters can be used instead of the unmodified values in the equation for Δx. It must however be noted that the compression model only holds when $\nu_P \leq 0.5$ as otherwise negative values for ν_P^* will be predicted.

$$\Delta x^* = \frac{t}{1-R}\left(\frac{t^2}{b^2(R-1)^2(R-2)^2}+1\right)^{-\frac{1}{2}} \tag{10a}$$

$$\approx b\sin(\alpha) \tag{10b}$$

It should be noted that the compaction model is only valid for the approximation of the membrane thickness. Due to the complex hydrostatic equilibrium achieved during the consolidation of the tapes, as well as the deviation of the overall arrangement of the tapes from the idealised model, the compaction modelling cannot be directly applied to all variables. When compaction is applied to all variables the models significantly under-predicted the mean permeability P_x, while only applying compaction to the membrane thickness Δx shows considerably better agreement with the experimental findings.

2.2. Permeability coefficients

From Eq. (6) all parameters, aside from the permeability coefficients P_γ and P_ξ, are known as they arise from the geometry of the tapes.

The permeabilities P_γ and P_ξ are determined via mixture rules for parallel and series arrangements respectively [25]. For this, the volume content ν_P is used to define the amount of permeable material there is in each 'tape'. The permeability of the polymer and metal are denoted by P_P and P_M respectively.

The tapes are manufactured in one of two ways. The first method employs vapour deposition to deposit a metal film on the thermoplastic polymer. In this process, the metallic layer grows from numerous nucleation sites on the polymer film, which then merge into one another. At these boundaries, the metallic layer is not perfectly crystalline and as such not perfectly impermeable. This was observed by Ref. [26].

Alternatively, a laminating process is used by applying a pure metal film to a thermoplastic film using an adhesive. This type of laminated film has significantly fewer defects as the metal layer is thicker and consists of a homogeneous material. With increasing aluminium thickness flaws become less frequent, until the product is no longer prone to pinholing [27]. This critical value is reached after 17μm [27,28].

It is assumed that these flawed boundaries are small in comparison to the metal crystals. Furthermore, it is assumed that these flaws are randomly and evenly distributed across the impermeable surface of the tape. Consequently, the flaw term ϕ must be determined experimentally to accurately model the diffusion through the tapes.

If the impermeable layer has no faults $P_\xi = 0$; however, as this layer is very thin, flaws cannot be avoided. For this reason, flaws are accounted for by introducing the term ϕ, which indicates how much of the impermeable layer is incomplete and filled with the permeable material. A schematic representation of the flaws is shown in Fig. 2.

$$\mathrm{P}_\gamma = \nu_\mathrm{P} P_P + (1-\nu_P) P_M \tag{11a}$$

$$P_\xi = \left(\frac{\nu_p}{P_P} + \frac{1-\nu_P}{(1-\phi)P_M + \phi P_P}\right)^{-1} \tag{11b}$$

2.3. Multiple layers

The effects of stacking and combining multiple membranes with overlapping tapes have also been explored. These angled tapes increase the effective diffusion path. The use of multiple layers allows this effective diffusion path to be increased even more without increasing the barrier membrane thickness significantly. This means multiple layers can be used without impacting the volumetric efficiency of a pressure vessel employing a barrier membrane manufactured in this way.

The number of layers L and their respective shift ω to the previous layer are further parameters available to the engineer for the design and optimisation of the barrier layer leakage tightness. Assuming that due to the induced angle α there is a defined and predictable path, the influence on the mean permeability can be estimated by modifying the diffusion path in the γ- direction.

$$P_x \approx L\Delta x\left(P_\gamma \frac{\sin(\alpha)}{Rb + (L-1)b\omega} + P_\xi \frac{\cos^2(\alpha)}{L\Delta x}\right) \tag{12}$$

This demonstrates that the addition of multiple layers not only increases the total membrane thickness, but also reduces the mean permeability of the multi-layer membrane. As such, it is highly beneficial to incorporate multiple layers.

3. Material and method

3.1. Material and experiment

Numerous experiments were performed to accompany the analytical and finite element models. All samples were manufactured from a three-

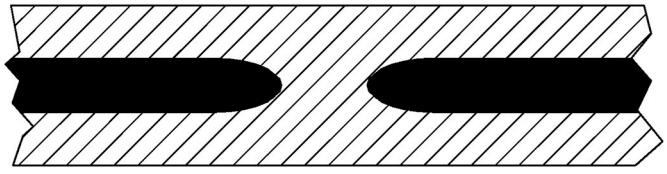

Fig. 2. Schematic representation of flaw in the impermeable layer (solid). The flaw is filled with the permeable material (hatched). These flaws are small in comparison to the impermeable crystals and are randomly and evenly distributed across the tape surface.

layer material.

For all samples, the polymer phase is polypropylene and the inner metallic film is made of EN-AW-1050A aluminium with a purity of 99.5%. These layers are held together by a thin adhesive film (HMF200), which was not modelled in the finite element simulations. The tapes were manufactured to have an aluminium thickness of 50μm and a polypropylene film with a thickness of 40μm on either side.

Samples were manufactured by manually stacking the tapes with width of 10mm and consolidated using an out-of-autoclave process at a temperature above the melting temperature of the polymers, exploiting the heat sealing capability of the tapes as explored in Ref. [29]. A simple vacuum bagging process was used to consolidate the tapes during this process. Samples were subsequently cut to size and placed in the permeation test stand.

Permeation tests were performed at a sample level by separating two volumes with the membranes. In one volume, a set helium pressure is applied and in the other, a leak detector detects permeating helium using sector mass spectrometry.

For these tests, a rectangular flange was manufactured to explore the effects of overlapping tapes. The flange has a rectangular hole with dimensions of 40 × 40mm. A pressure difference Δp of 1 bar was used for all tests to avoid deforming the thin membranes. At elevated pressures the permeability of the polymer may be negatively influenced and must therefore be determined at use case conditions before being used in the models presented. Despite the potential deterioration of the polymer properties the ratio of the membrane permeability and the polymer permeability is preserved, as it is purely a consequence of the tape and membrane geometry. Thus, the membrane will maintain its efficiency over pure polymeric liners. The flange and sample are shown in Fig. 3.

The measurement area for each overlap ratio had to be determined specifically as not all tapes inside the total measurement area offer a diffusion path. This specific area A^* is composed of the number of effective diffusion paths n, the width of the RVE w and the width of the flange F.

$$A^* = nwF \tag{13}$$

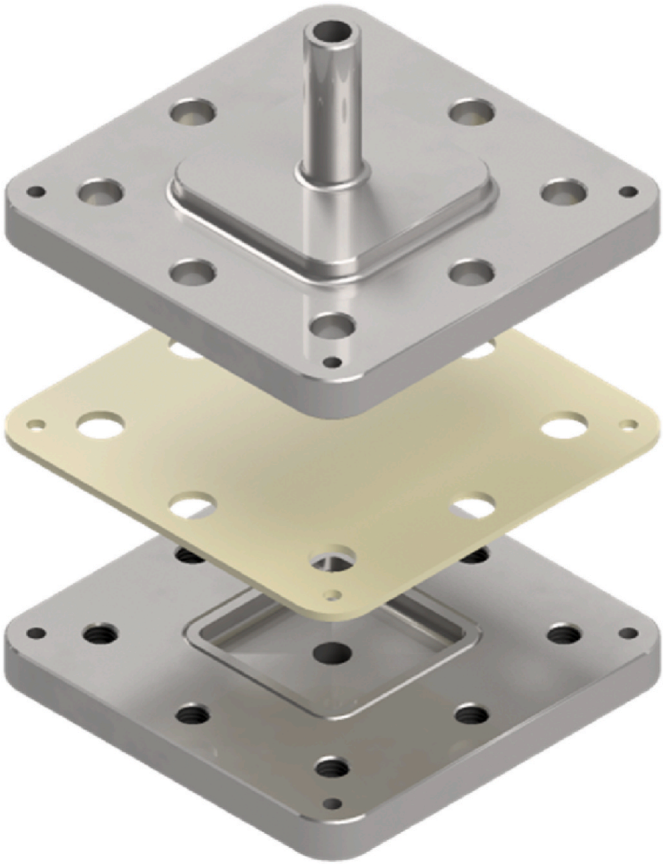

Fig. 3. Representation of diffusion test flange and sample in an exploded view. On the bottom flange the measurement area and v-cut for an indium seal are visible. Samples and Flanges have holes for fastening bolts.

3.2. Finite element models

Two-dimensional finite element models (FEM) were set up in *Abaqus* to compare against the novel analytical model. The finite element models solve the diffusion equation which describes the macroscopic behaviour of particles. Hence, merely the material properties, namely the diffusivity and solubility, have to be defined for the polymer and metal. These properties were determined experimentally for the neat polymer material. The geometries for the finite element model were constructed based on the idealised geometry shown in Fig. 1, thereby allowing a simple parametric approach to the modelling of the membrane. Compaction was not included in the modelling as the resulting internal arrangement of the materials cannot easily be predicted. A representative volume element (RVE) model is used to simulate the membrane.

The boundary conditions can be divided into two groups: the boundary conditions arising from the intrinsic assumptions of the diffusion process applied to the faces of the membrane, and the periodic boundaries through the thickness of the membrane at the edges of the RVE.

The boundary on the pressure face is defined via Henry's law (Eq. (14)) to determine the concentration at the face based on the pressure of the detector gas. Similarly, the concentration of the permeating gas at the detector face can be defined via Henry's law where the pressure is zero.

$$c = Sp \tag{14}$$

Periodic boundary conditions were implemented to ensure that the concentrations on the left and right sides of the model remained equal for each pair of nodes throughout the thickness. This allows concentration changes occurring on either side to be reflected on the other. By applying these periodic boundary conditions, the FEM model can simulate the behaviour of the layered tapes with periodicity. Eq. (15) holds for the left and right edges of the model.

$$c_{i,\text{Left}} - c_{i,\text{Right}} = 0 \tag{15}$$

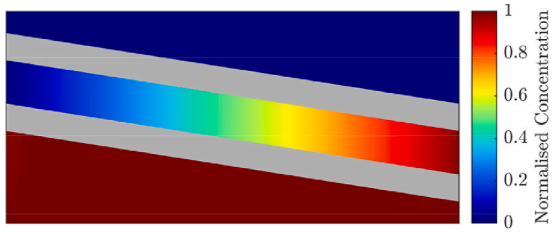

(a) Detailed image of single RVE.

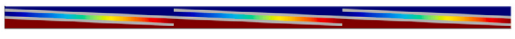

(b) Multiple RVEs showing repeating pattern.

Fig. 4. Concentration results through the membrane for RVE model. High and low concentrations are at the pressure and detector face respectively, which are connected by a linear transition between the aluminium tapes, shown in grey. Note: figures are to show detail and are not to scale.

3.2.1. Extracting permeability from FEM simulations

The finite element models (see Fig. 4) show that the concentration through the thickness of the membrane is not uniform. Due to the impermeable nature of the metallic barriers, the lower section of the membrane is almost fully saturated, while a linear decrease in the concentration can be observed in the overlapping regions of the tapes. From here, the diffusion problem is similar to a point source where the concentration spreads out in bands.

The overlapping nature of the tapes results in a non-uniform concentration gradient at the boundary, where the concentration cyclically spikes where the overlapping tape ends and the gas is free to diffuse without obstruction.

The concentration data obtained from the FEM analysis can be utilized in conjunction with Eq. (1) to determine the total leak rate. The total leak rate can be determined by integrating the dot product of the flux vector **J** and the normal vector **n** over the surface of the membrane, as shown in Eq. (16). Substituting Eq. (1) yields the surface integral of the dot product of the concentration gradient at the membrane boundary and the normal vector multiplied by the diffusivity of the polymer.

$$Q = \iint_S \mathbf{J}\cdot\mathbf{n}\, dS = -D\iint_S \nabla c\cdot\mathbf{n}\, dS \tag{16}$$

This may be rearranged to derive the permeability P_x for the membrane unit cell, as shown in Eq. (17).

$$P_x = \frac{1}{A}\left(\frac{\Delta p}{\Delta x}\right)^{-1}\iint_S \mathbf{J}\cdot\mathbf{n}\, dS \tag{17}$$

3.3. Research methodology

Three avenues were pursued to motivate, develop and verify the barrier membrane concept. The analytical model was developed to indicate the potential of the concept and allow an overall insight into the effects of manufacturing parameters. Finite element models were developed to understand the diffusion behaviour through individual diffusion paths. Lastly experimental tests were carried out to verify the model predictions. For this multiple identical samples were manufactured and tested to add statistical significance to experimental findings. The leak rate values were converted to the mean permeability P_x and compared to other model predictions.

4. Results and discussion

4.1. Micrograph analysis

Micrograph sections were made to explore the true layout of the tapes and confirm the thickness of each layer. This is exemplified in Fig. 5. As demonstrated the true layout of the tapes differs from the idealised model. The tapes adopt an elongated S-shaped form, as opposed to flat, angled tapes. However, due to the high aspect ratio of the tapes and the slight undulations arising from the manufacturing process, the overall geometry can still be approximated with the idealised model. Despite the difference in the assumed shape of tapes in the laminate, the total thicknesses are in agreement with one another, as is shown in Table 1, however, the compaction in the consolidation phase must be taken into account for future developments. This may be attributed to the complex hydrostatic equilibrium during the consolidation phase.

The comparison of membrane thickness according to the theoretical predictions and the experimental results shown in Table 1, suggests that during the consolidation of the membrane, a considerable portion of the polymer is squeezed out to fill the triangular notches. This reduces the portion of permeable material resulting in a further improvement of the permeability.

4.2. Permeation tests

Permeation tests of layered tapes were performed to validate the analytical and finite element models. Measurements were run until the leak rate had reached a steady state. The diffusion process is demonstrated in Fig. 6. The flux curves demonstrate that higher overlap ratios take longer to reach a steady-state condition, which is in line with the theoretical predictions. Contrary to the model predictions, the flux values increase with overlap ratios, suggesting that effects at the edges of the test samples artificially reduce the leak rate through outer diffusion paths.

A schematic representation of the sample mounted in the diffusion flange is shown in Fig. 7. The tape geometry is distorted for clarity. The bottom flange holds the test gas, while the top flange is connected to a leak detector. Due to the arrangement of the tapes the left most RVEs and their associated diffusion paths are exposed on the bottom flange to the test gas but redirect the flux away from the detector face into the top flange. Similarly, the right-most RVEs entering the detector face are blocked on the bottom face by the flange. Therefore, the left and right

Table 1
Comparison of membrane thickness estimation with and without compaction against experimental data for different levels of overlap R. Repeated measurements were taken with a micrometre and averaged. *An overlap ratio of $R = 0.9$ was intended, but could not be achieved during manufacturing.

Overlap	Thickness Δx (mm)		
R	Analytical	Compaction	Micrograph
0.25	0.303	0.173	0.168
0.50	0.390	0.260	0.275
0.75	0.649	0.520	0.540
0.87*	1.156	1.026	1.026

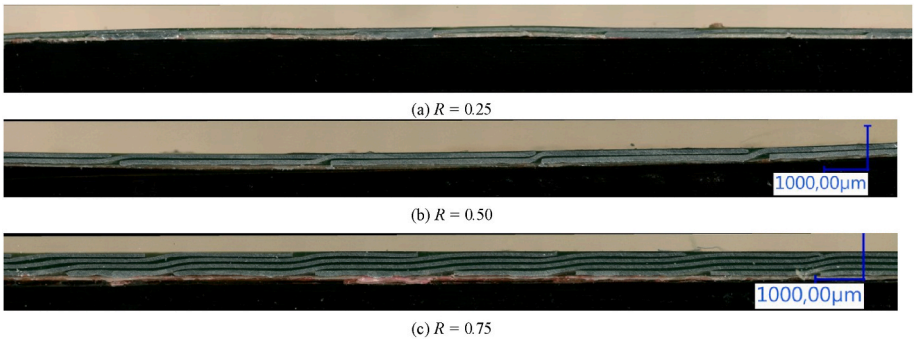

(a) $R = 0.25$

(b) $R = 0.50$

(c) $R = 0.75$

Fig. 5. Micrograph section of membrane manufactured with overlapping tapes at x1000 magnification, demonstrating that individual tapes do not strongly deviate from the idealised model. Micrographs of samples with an overlap of $R = 0.87$ could not be obtained, as samples were plastically deformed after extraction from the test flange.

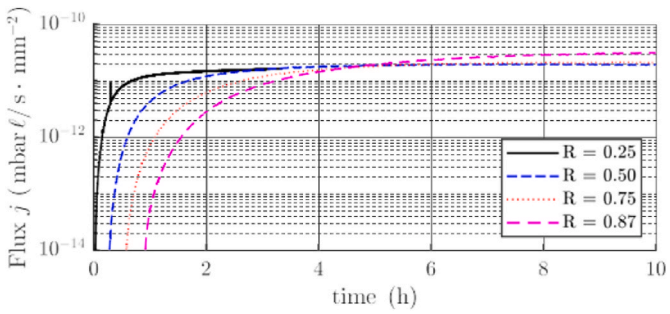

Fig. 6. Flux over time for all overlap ratios normalised with the estimated area A^*. Increased overlap ratios demonstrate higher steady-state flux results while taking longer to reach a steady state.

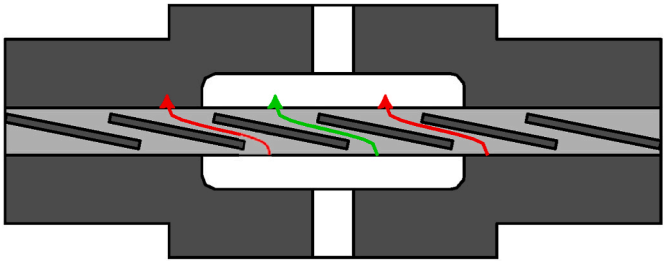

Fig. 7. Schematic representation of sample mounted in test flange. The flanges are shown in dark grey. The polymer of the sample is represented in light grey and the aluminium foil is represented in dark grey. The tape geometry is not to scale for simplicity. Red and green arrows represent obstructed and unobstructed diffusion paths respectively. (For interpretation of the references to colour in this figure legend, the reader is referred to the Web version of this article.)

RVEs do not contribute to the total leak rate. As such the number of diffusion paths in the test flange is influenced by the tape geometry. Due to the aforementioned effects, accurately predicting the total area is challenging, and even Eq. (13) offers only an estimate.

The analytical model with and without compaction, finite element model and experimental results are shown in Fig. 8. Error bars are included for the experimental results for both the overlap ratio R and the mean permeability P_x to indicate the measurement uncertainties. The mean permeability is normalised by the permeability of pure polymer (polypropylene).

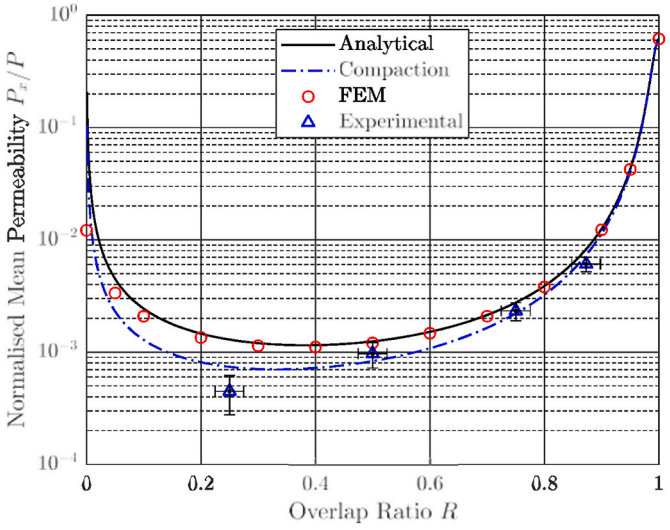

Fig. 8. Comparison of analytical, finite element and experimental results for layered tapes with varying overlap ratio R. Tapes are manufactured with a constant width b of 10 mm. Data points represent mean values for test conditions. Error bars for experimental results indicate measurement uncertainties arising from the manufacturing process and test equipment.

The larger discrepancies for low overlap ratios between the experimental findings and the theoretical predictions can be explained by the effect previously discussed where the RVEs at the edges of the test area are partially or fully obstructed by the flange.

The analytical model and the finite element models are in considerable agreement with one another. Only at very low overlap ratios R do the finite element results depart from the idealised model. However, for meaningful overlap ratios that can be realised in a winding process, both approaches demonstrate significant reductions in the membrane permeability. Additionally, the analytical model is slightly more conservative than the finite element predictions. As such the novel analytical model is validated.

The experimental results align well with analytical predictions with compaction. This validates the simplified models created. However, the notable discrepancies in the flux and permeability results, particularly for low overlap ratios, suggest that larger samples must be manufactured and tested such that the artificial leak rate reductions at the edges of the sample become negligible.

4.3. Model application and outlook

The performance of this barrier membrane concept may be further increased by optimising the materials used. As such the two variables that can be modified are the polymer fraction ν_P and aspect ratio $\mathscr{AR}$. The overlap R can be subsequently determined for optimal permeability reductions. With a reduction of the polymer fraction from 0.61 (this study) to 0.5 the permeability of the barrier membrane is 2960 times better than that of pure polymer. Further increasing the aspect ratio 200 improves the permeability by a factor of 11 850. This is shown in Fig. 9.

5. Conclusion

The models developed in addition to the experimental results suggest that a wound barrier membrane with over-lapping tapes lends itself to applications in carbon fibre-reinforced pressure vessels. For a single layer, the mean permeability may be reduced by several orders of magnitude compared to a pure polymer. Furthermore, with the addition of multiple layers and the associated reduction in the permeability and

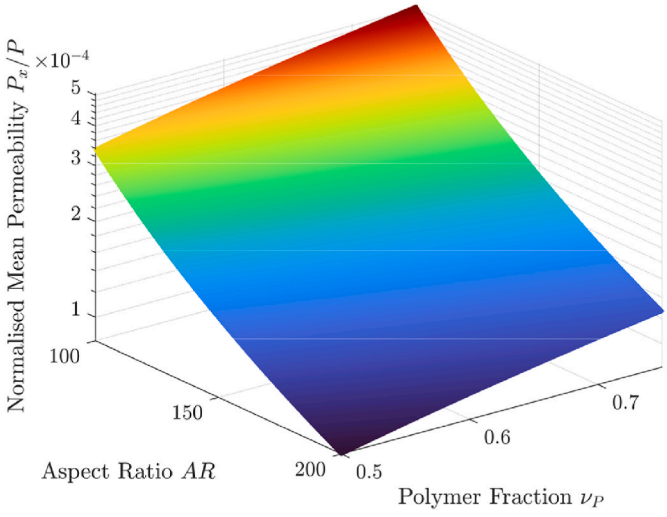

Fig. 9. Parameter study of barrier membrane concept based on novel analytical model with compaction. For each combination of aspect ratio $\mathscr{AR}$ and polymer fraction ν_P the overlap ratio R is optimised for minimal permeability.

increase in membrane thickness, strict impermeability requirements can be met for aerospace applications. Through the appropriate selection of the tape geometry kinking may be minimised during the winding process of the barrier membrane.

The experimental tests performed herein only served as a validation of the models. Consequently, the permeability reductions although significant did not meet the full potential. There is significant optimisation potential in the composition and geometric arrangement of the tapes for significant improvements in leak tightness and processability. As was noted, the concentration gradient is highly non-uniform across the unit cell. It is therefore hypothesized that a crude simplification to the mean permeability is only valid for a single layer and that the inclusion of further layers with strategic placement can improve the leak rate beyond the simple model described herein. This will require further investigation to explore the effects of multiple layers of overlapping tapes on the permeability.

The tapes investigated have a uniform width to be integrated in a winding process. Alternatively, the membrane material can be segmented into larger sheets, resulting in a more efficient barrier membrane structure at the cost of a more intensive manufacturing process. Here the permeation model developed in this publication may be adapted to model single overlaps instead of a repeated structure.

Declaration of competing interest

The authors declare that they have no known competing financial interests or personal relationships that could have appeared to influence the work reported in this paper.

CRediT authorship contribution statement

Nico Gerster: Writing – review & editing, Writing – original draft, Visualization, Validation, Software, Methodology, Investigation, Formal analysis, Data curation, Conceptualization. **Andreas Scherer:** Writing – review & editing, Investigation. **Gerrit Rehs:** Writing – review & editing, Resources, Investigation. **Tobias Dickhut:** Writing – review & editing.

Acknowledgements

The material was supplied by *Gemet GmbH technical adhesive foils*.

This work was supported by the dtec.bw -Digitalization and Technology Research Center of the Bundeswehr through the Project SeRANIS - Seamless Radio Access Networks in the Internet of Space under Grant 150009910 and CHiLL - Cryogenic Helium-Tanks in Low-Cost Linerless-Technology under Grant 50RK2142 and CryoFuselage under Grant LABAY108B.

References

[1] Usman MR. Hydrogen storage methods: review and current status. Renew Sustain Energy Rev 2022;167:112743. https://doi.org/10.1016/j.rser.2022.112743. https://www.sciencedirect.com/science/article/pii/S1364032122006311.

[2] Barthelemy H, Weber M, Barbier F. Hydrogen storage: recent improvements and industrial perspectives. Int J Hydrogen Energy 2017;42(11):7254–62. https://doi.org/10.1016/j.ijhydene.2016.03.178.

[3] Schultheiß D. Permeation barrier for lightweight liquid hydrogen tanks. Augsburg University; 2007. Ph.D. thesis.

[4] Air A, Shamsuddoha M, Gangadhara Prusty B. A review of type v composite pressure vessels and automated fibre placement based manufacturing. Compos B Eng 2023;253:110573. https://doi.org/10.1016/j.compositesb.2023.110573. https://www.sciencedirect.com/science/article/pii/S1359836823000768.

[5] Ogasawara T, Arai N, Fukumoto R, Ogawa T, Yokozeki T, Yoshimura A. Titanium alloy foil-inserted carbon fiber/epoxy composites for cryogenic propellant tank application. Adv Compos Mater 2014;23. https://doi.org/10.1080/09243046.2013.844756.

[6] Azeem M, Ya HH, Alam MA, Kumar M, Stabla P, Smolnicki M, Gemi L, Khan R, Ahmed T, Ma Q, Sadique MR, Mokhtar AA, Mustapha M. Application of filament winding technology in composite pressure vessels and challenges: a review. J Energy Storage 2022;49:103468. https://doi.org/10.1016/j.est.2021.103468. https://www.sciencedirect.com/science/article/pii/S2352152X2101152X.

[7] Ma Q, Rejab M, Azeem M, Hassan SA, Yang B, Kumar AP. Opportunities and challenges on composite pressure vessels (cpvs) from advanced filament winding machinery: a short communication. Int J Hydrogen Energy 2024;57:1364–72. https://doi.org/10.1016/j.ijhydene.2024.01.133. https://www.sciencedirect.com/science/article/pii/S0360319924001368.

[8] Su Y, Lv H, Zhou W, Zhang C. Review of the hydrogen permeability of the liner material of type iv on-board hydrogen storage tank. World Electric Vehicle Journal 2021;12(3):130. https://doi.org/10.3390/wevj12030130.

[9] Condé-Wolter J, Ruf MG, Liebsch A, Lebelt T, Koch I, Drechsler K, Gude M. Hydrogen permeability of thermoplastic com- posites and liner systems for future mobility applications. Compos Appl Sci Manuf 2023;167:107446. https://doi.org/10.1016/j.compositesa.2023.107446.

[10] Humpenöder J. Gas permeation of fibre reinforced plastics. Cryogenics 1998;38(1):143–7. https://doi.org/10.1016/S0011-2275(97)00125-2. https://www.sciencedirect.com/science/article/pii/S0011227597001252.

[11] Murray BR, Leen SB, Semprimoschnig CO, Brádaigh CM. Helium permeability of polymer materials as liners for composite overwrapped pressure vessels. J Appl Polym Sci 2016;133(29). https://doi.org/10.1002/app.43675.

[12] Fang Q, Ji D. Molecular simulation of hydrogen permeation behavior in liner polymer materials of type iv hydrogen storage vessels. Mater Today Commun 2023;35:106302. https://doi.org/10.1016/j.mtcomm.2023.106302. https://www.sciencedirect.com/science/article/pii/S2352492823009935.

[13] Jung J, Kim I, Kim K. Evaluation of hydrogen permeation characteristics in rubbery polymers. Curr Appl Phys 2021;21:43–9. https://doi.org/10.1016/j.cap.2020.10.003. https://www.sciencedirect.com/science/article/pii/S1567173920302303.

[14] Kanesugi H, Ohyama K, Fujiwara H, Nishimura S. High-pressure hydrogen permeability model for crystalline polymers. Int J Hydrogen Energy 2023;48(2):723–39. https://doi.org/10.1016/j.ijhydene.2022.09.205. https://www.sciencedirect.com/science/article/pii/S036031992204441X.

[15] Kumar M. Investigation of hydrogen transport properties through the liner material of 70 mpa type iv composite overwrapped pressure vessels. Int J Pres Ves Pip 2024;208:105150. https://doi.org/10.1016/j.ijpvp.2024.105150. https://www.sciencedirect.com/science/article/pii/S0308016124000279.

[16] Cussler E, Hughes SE, Ward WJ, Aris R. Barrier membranes. J Membr Sci 1988;38(2):161–74. https://doi.org/10.1016/S0376-7388(00)80877-7. https://www.sciencedirect.com/science/article/pii/S0376738800808777.

[17] Derocher J, Gettelfinger B, Wang J, Nuxoll E, Cussler E. Barrier membranes with different sizes of aligned flakes. J Membr Sci 2005;254(1–2):21–30. https://doi.org/10.1016/j.memsci.2004.12.025.

[18] Habel C, Tsurko ES, Timmins RL, Hutschreuther J, Kunz R, Schuchardt DD, Rosenfeldt S, Altstädt V, Breu J. Lightweight ultra-high-barrier liners for helium and hydrogen. ACS Nano 2020;14(6):7018–24. https://doi.org/10.1021/acsnano.0c01633.

[19] Lu Z, Zhou Q, Zhang Y, Atya A, Zhang T, Zhang G, Zhang Y, Liu G, Jiang W, Hu Y. Enhanced gas and plasticizer barrier htpb com- posite liner implanted with parallel orientation fe3o4/rgo nanosheets by an ultrasound/magnet-coassisted method. Ultrason Sonochem 2024;104:106827. https://doi.org/10.1016/j.ultsonch.2024.106827. https://www.sciencedirect.com/science/article/pii/S1350417724000750.

[20] Yan Y, Zhang J, Li G, Zhou W, Ni Z. Review on linerless type v cryo-compressed hydrogen storage vessels: resin toughening and hydrogen-barrier properties control. Renew Sustain Energy Rev 2024;189:114009. https://doi.org/10.1016/j.rser.2023.114009. https://www.sciencedirect.com/science/article/pii/S1364032123008675.

[21] Cheng S, Hassan A, Ghazali MI, Ismail A. Heat sealability of laminated films with lldpe and ldpe as the sealant materials in bar sealing application. J Appl Polym Sci 2007;104:3736–45. https://doi.org/10.1002/app.25863.

[22] Anderson L, Kemp B. Metallised packaging films in the us market. In: 3rd ICI European metallising symposium; 1978. Venice.

[23] Fick A, on liquid diffusion V. London, Edinburgh Dublin Phil Mag J Sci 1855;10(63):30–9. https://doi.org/10.1080/14786445508641925.

[24] William H. Iii. experiments on the quantity of gases absorbed by water, at different temperatures, and under different pressures. Phil Trans Roy Soc Lond 1803;93:29–274. https://doi.org/10.1098/rstl.1803.0004.

[25] Solovyov SE, Goldman AY. Permeability of multi-layer structures. E-Polymers Dec 2004;4(1). https://doi.org/10.1515/epoly.2004.4.1.234.

[26] Mercea P, Muresan L, Mecea V. Permeation of gases through metallized polymer membranes. J Membr Sci 1985;24(3):297–307. https://doi.org/10.1016/S0376-7388(00)82247-4. https://www.sciencedirect.com/science/article/pii/S0376738800822474.

[27] Murray L. The impact of foil pinholes and flex cracks on the moisture and oxygen barrier of flexible packaging. In: TAPPI PLACE conference, las vegas. Nevada; 2005.

[28] Kerry J. 9 - aluminium foil packaging. In: Emblem A, Emblem H, editors. Packaging technology. Woodhead Publishing; 2012. p. 163–77. https://doi.org/10.1533/9780857095701.2.163. https://www.sciencedirect.com/science/article/pii/B9781845696658500093.

[29] Meka P, Stehling FC. Heat sealing of semicrystalline polymer films. i. calculation and measurement of interfacial temperatures: effect of process variables on seal properties. J Appl Polym Sci 1994;51(1):89–103. https://doi.org/10.1002/app.1994.070510111.